Check for updates

ADVANCED MATERIALS
www.advmat.de

Design Strategy for Transformative Electronic System toward Rapid, Bidirectional Stiffness Tuning using Graphene and Flexible Thermoelectric Device Interfaces

Sang-Hyuk Byun, Choong Sun Kim, Karen-Christian Agno, Simok Lee, Zhuo Li, Byung Jin Cho, and Jae-Woong Jeong**

Electronics with tunable shape and stiffness can be applied in broad range of applications because their tunability allows their use in either rigid handheld form or soft wearable form, depending on needs. Previous research has enabled such reconfigurable electronics by integrating a thermally tunable gallium-based platform with flexible/stretchable electronics. However, supercooling phenomenon caused in the freezing process of gallium impedes reliable and rapid bidirectional rigid–soft conversion, limiting the full potential of this type of "transformative" electronics. Here, materials and electronics design strategies are reported to develop a transformative system with a gallium platform capable of fast reversible mechanical switching. In this electronic system, graphene is used as a catalyst to accelerate the heterogeneous nucleation of gallium to mitigate the degree of supercooling. Additionally, a flexible thermoelectric device is integrated as a means to provide active temperature control to further reduce the time for the solid–liquid transition of gallium. Analytical and experimental results establish the fundamentals for the design and optimized operation of transformative electronics for accelerated bidirectional transformation. Proof-of-concept demonstration of a reconfigurable system, which can convert between rigid handheld electronics and a flexible wearable biosensor, demonstrates the potential of this design approach for highly versatile electronics that can support multiple applications.

Conventional electronics are manufactured with high stiffness to make them suitable for easy handling and robust interfacing. On the contrary, emerging soft electronics are developed with high degree of freedom and surface-compliantness to optimize their features for wearable and implantable applications.[1–8] Although they are highly useful and reliable for their targeted uses, the static form factor of both rigid and soft electronics limits broad utility beyond their designated applications. To take full advantage of the essential characteristics of both rigid and soft electronics, a new class of electronics, which can tune their shape and stiffness, has been developed by integrating a temperature-responsive transformative platform with flexible and stretchable electronics.[9,10] This type of electronic device, herein referred to as a transformative electronics system (TES), maintains its rigid form in a handheld or tabletop setup at room temperature, but the device structure softens at physiological temperature when attached onto the skin, thereby allowing conformal and comfortable integration with the body.

To enable temperature-dependent reconfiguration, the initial TES development utilized gallium (Young's modulus: 9.8 GPa in solid; melting temperature: 29.76 °C) as a core material for the transformative platform, which offers large elastic modulus tuning (10 s kPa to 100 s MPa) through changing the gallium state between solid and liquid. Although a gallium-based TES has shown promise to broaden the applications of electronics by enhancing versatility through rigid–soft mode conversion, achieving rapid bidirectional transformation has been an arduous undertaking mainly due to the supercooling phenomena of gallium, which leads to a significant delay in phase transition in soft-to-rigid conversion. To realize the full potential of TES with fast bidirectional rigid–soft transformation capability, it is necessary to overcome the issue of supercooling in the gallium-based TES.[9,11]

Several approaches have been investigated to solve the supercooling issue during the phase change of a material from liquid to solid state. Electrofreezing[12] and mechanical stimulation[13,14] have been shown to reduce the degree of supercooling; however, these methods reportedly show unstable supercooling reduction and requires an external device for electric stimulation or

S.-H. Byun, C. S. Kim, K.-C. Agno, S. Lee
School of Electrical Engineering
Korea Advanced Institute of Science and Technology (KAIST)
Daejeon 34141, Republic of Korea
Prof. Z. Li
Department of Materials Science
Fudan University
Shanghai 200433, China
Prof. B. J. Cho, Prof. J.-W. Jeong
School of Electrical Engineering
Korea Advanced Institute of Science and Technology (KAIST)
Daejeon 34141, Republic of Korea
E-mail: bjcho@kaist.edu; jjeong1@kaist.ac.kr
The ORCID identification number(s) for the author(s) of this article can be found under https://doi.org/10.1002/adma.202007239.

DOI: 10.1002/adma.202007239

 © 2021 Wiley-VCH GmbH

mechanical shock that is not appropriate to enable a compact design. Adding nucleating agents (e.g., TeO2, CaO, MgO, Fe, and Cu) can accelerate the nucleation of gallium,[11] but the reduction in the degree of supercooling has been revealed to be inconsistent, failing to provide a constant, controllable phase transition time. In addition, gallium-coated copper is known to induce heterogeneous nucleation of liquid metal,[15] but its catalytic effect has not been studied in depth. Alternatively, instead of trying to decrease the degree of supercooling, a sufficiently low temperature (e.g., <5 °C) can be applied through circulation of water coolant to effectively and rapidly cool down the phase change material to overcome the supercooling.[16] Although the lower temperature drives relatively faster liquid-to-solid transition, this approach requires a bulky chiller to keep the water cold, thus making it an undesirable option for TES.

As a solution to enable rapid bidirectional transformation of TES, we report a TES built on a gallium platform integrated with graphene and a flexible thermoelectric device (f-TED). Here graphene interfaced with gallium, which gives rise to a catalytic effect in liquid-to-solid conversion, lowers the degree of supercooling by providing large area of preferential sites to facilitate nucleation. Additionally, the f-TED offers active temperature control to accelerate the solid–liquid phase transition of gallium with elevated or lowered temperature, thus supporting speedy conversion of the TES from the rigid to soft mode or vice versa. Due to its compact design and capability of fast mechanical mode switching, this system may open new opportunities for various personal electronics, robotics, and biomedical devices. The following section presents theoretical analysis and experimental characterization of graphene-induced heterogeneous nucleation of gallium and their application to construct an f-TED-integrated TES capable of fast, bidirectional rigid–soft mode conversion. Successful demonstration of a TES that can rapidly convert between a rigid handheld display and a flexible wearable pulsimeter/display illustrates the potential utility of this design approach to realize highly versatile multipurpose electronics.

Figure 1a shows a conceptual illustration of a TES that is switchable between a rigid handheld display and a wearable pulsimeter, highlighting reinforced rapid rigid–soft mode conversion enabled by the integration of graphene and an f-TED with a gallium-based transformative platform. More specifically, this exemplary transformative optoelectronics device consists of flexible optoelectronics with light-emitting diodes (LEDs) and photodetectors (PD), a transformative platform built with a graphene-coated gallium frame with silicone encapsulation, and an f-TED. In this design, graphene and the f-TED play a critical role to accelerate bidirectional mechanical mode conversion by helping to overcome the supercooling issue that appeared during soft-to-rigid transition in a previously reported TES[9] as well as by shortening the phase transition time in rigid-to-soft switching. The ultrathin nature of graphene, which is a single layer of carbon atoms in a two-dimensional structure, not only facilitates its conformal lamination onto the gallium structure, but also provides an ultrahigh specific surface area,[17] thereby providing numerous nucleation sites over a large area that allow faster triggering of solidification of liquid gallium during the freezing process, compared to one-dimensional carbon-based material (e.g., graphite; Figure S1, Supporting Information). With the reduced degree of supercooling through the graphene-assisted nucleation, the supercooled state becomes considerably shortened in the phase transition, thus significantly reducing the time necessary for transformation of the TES to the rigid mode in comparison to the time required to freeze pure liquid gallium. This soft-to-rigid transition time can be further decreased by actively lowering the gallium temperature using the integrated f-TED. In a similar way, the f-TED can enable acceleration of rigid-to-soft mode conversion through artificial heating-up of the transformative platform, facilitating rapid bidirectional mode switching of the TES.

Figure 1b illustrates the principle of accelerated solidification of liquid gallium that can be enabled by the introduction of graphene interfacing as a means to address the supercooling phenomenon in the freezing process. During liquid-to-solid transition, gallium should overcome a thermodynamic barrier called the nucleation barrier (ΔG^*, maximum free energy change) to initiate its crystallization, according to classical nucleation theory.[18] The key to faster solidification is lowering the nucleation energy barrier (ΔG^*), which can be achieved by decreasing the interfacial free energy and/or temperature (see Note S1 in the Supporting Information). In homogeneous nucleation with pure gallium, the only way to reduce ΔG^* is to apply a lower temperature, and this is the reason why pure gallium experiences a considerably large degree of supercooling before the phase change to solid. In the case of heterogeneous nucleation induced by graphene, however, a temperature as low as that required for homogeneous nucleation is not necessary to initiate nucleation because the interfacing of graphene with gallium significantly decreases ΔG^*. With the reduced degree of supercooling, the heterogeneous nucleation by graphene interfacing allows a faster transition from liquid to solid state compared to the homogeneous nucleation case. Figure 1c visually shows this catalytic effect of graphene associated with gallium solidification. According to infrared (IR) images taken during freezing at 0 °C, graphene-coated gallium reaches the freezing temperature faster for conversion to solid, whereas bare gallium still remains in the supercooled state, verifying accelerated phase change assisted by graphene.

Similarly, the capability of the f-TED to accelerate the bidirectional phase transition of gallium can be observed in the IR images shown in Figure 1d,e. Because the f-TED can actively and rapidly heat up or cool down the interface of the transformative platform, it can significantly shorten the time for the melting (Figure 1d) and freezing (Figure 1e) of gallium, compared to the case of relying on ambient temperature. Moreover, the f-TED assists to initiate the solidification by lowering the temperature to the nucleation temperature when the ambient temperature (≈22–25 °C) is not low enough to overcome the supercooling (top IR images (w/o f-TED), Figure 1e). For these reasons, the f-TED is another essential element for the TES to realize rapid rigid–soft mode conversion.

The experimental studies presented in **Figure 2** prove the effect of graphene as a catalyst in the heterogeneous nucleation of gallium. As seen in Figure 1b, nucleation can readily occur when the maximum free energy change (ΔG^*) is significantly reduced by decreasing the interfacial free energy (see Note S1 in the Supporting Information). The interfacial free energy between a liquid and a substance can be macroscopically

© 2021 Wiley-VCH GmbH

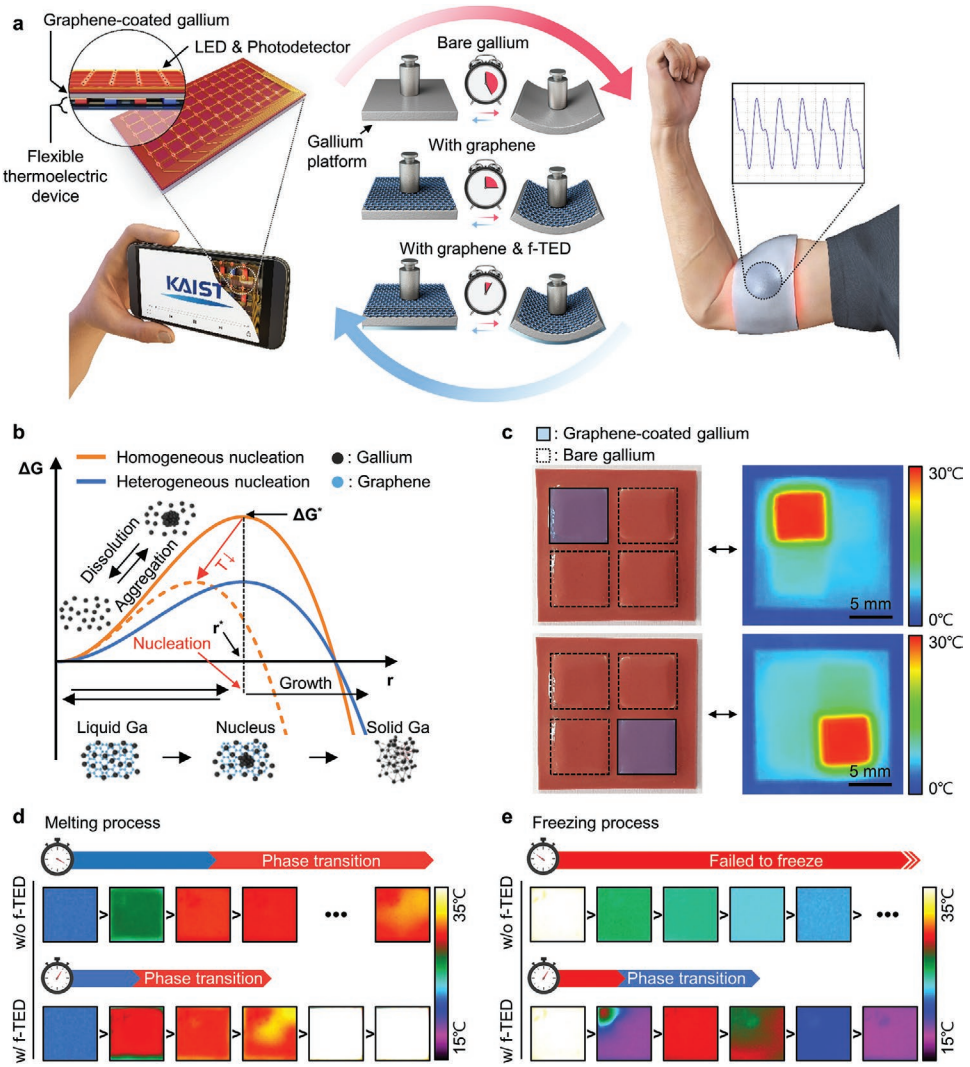

Figure 1. Overview of a transformative electronic system (TES) with bidirectional soft–rigid phase transition, accelerated by the integration of graphene and a flexible thermoelectric devices (f-TED) on a gallium-based platform. a) Schematic illustration of the key design concept of the TES for rapid bidirectional conversion between a rigid handheld electronic device and a soft wearable sensor. A transformative platform built with gallium, which relies on a temperature-dependent phase transition, can undergo reinforced rapid mode switching through interfacing with graphene and the f-TED. b) A conceptual plot illustrating the free energy change (ΔG) during the process of solidification of liquid gallium. Heterogeneous nucleation enabled by the integration of graphene decreases the required energy to initiate solidification, allowing faster transition of gallium from liquid to solid state. c) Optical images of polymer-encapsulated liquid gallium samples and corresponding infrared (IR) images taken during the phase transition, visually verifying that graphene enables faster triggering of gallium nucleation. The blue shaded boxes in the left images indicate the location of graphene-coated gallium. d,e) IR images illustrating the phase transition process of graphene-coated gallium without and with the f-TED during the melting (d) and freezing (e) processes. Both figures show that the f-TED substantially reduces the phase transition time for both melting and freezing of gallium.

determined using the contact angle (θ), according to Young's equation:[19] $\gamma_{LV}\cos\theta = \gamma_{SV} - \gamma_{SL}$, where γ_{LV}, γ_{SV}, and γ_{SL} represent the surface free energy of the liquid, the surface free energy of the substance, and the interfacial free energy, respectively (Figure 2a). The smaller the contact angle on the substance, the smaller the interfacial free energy between the liquid and the substrate it has, which makes the substance a good candidate as a catalyst for nucleation, i.e., nucleating agent. In addition, the wetting factor, $f(\theta)$, which is a function of the contact angle, provides the relationship between the contact angle and the nucleation energy barriers (i.e., $\Delta G^*_{het} = \Delta G^*_{hom} f(\theta)$, where ΔG^*_{hom} and ΔG^*_{het} represent nucleation barriers for homogeneous and heterogeneous nucleation, respectively).[20] A low contact angle translates to a low wetting factor which induces enhanced heterogeneous nucleation (Figure 2b). Thus, contact angle can be used as a key parameter for the performance evaluation of graphene in facilitating the heterogeneous nucleation of gallium.[21,22]

To measure the contact angle between liquid gallium and various materials, liquid gallium was dripped onto those substances. However, the formation of a thin oxide layer on the gallium surface impeded the flow of the liquid gallium, which led to stiction with the surface of a substrate material. To remove the oxide layer, liquid gallium was treated with hydrochloric

© 2021 Wiley-VCH GmbH

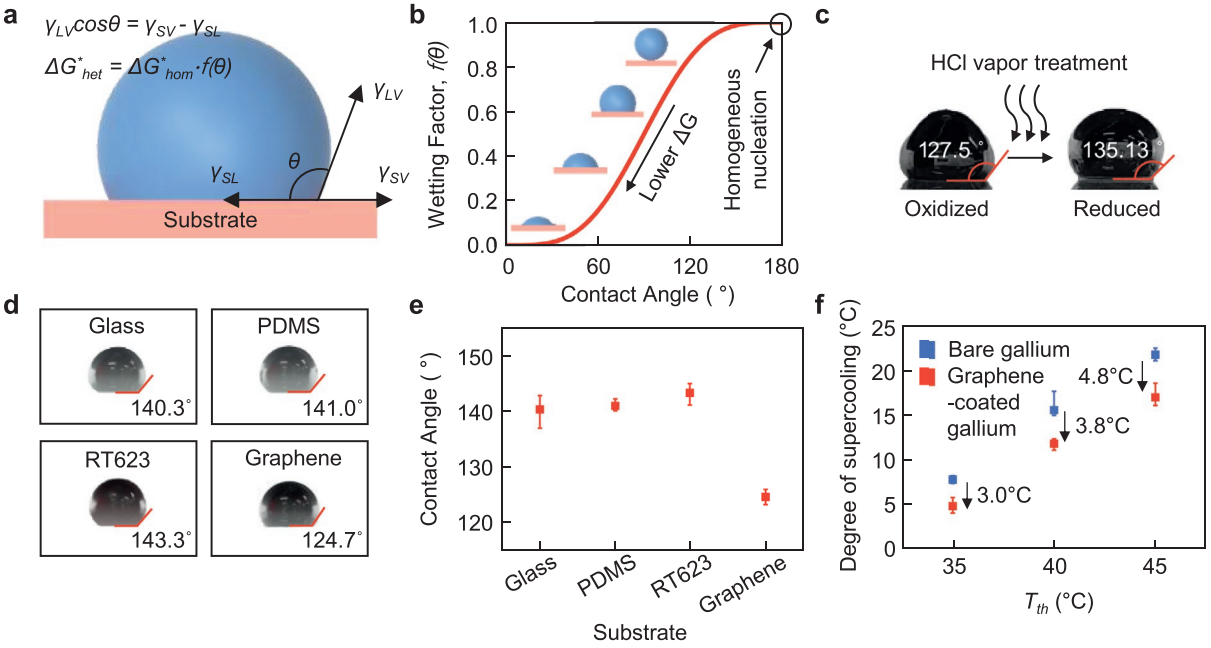

Figure 2. Interfacial mechanics of graphene leading to enhanced heterogeneous nucleation of gallium with alleviated degree of supercooling. a) Schematic diagram illustrating the relationship between interface energy, contact angle (θ), and free energy change (ΔG); γ_{LV}, γ_{SV}, and γ_{SL} are the surface free energy of liquid, the surface free energy of substance, and the interfacial free energy, respectively. Here, ΔG^*_{het} and ΔG^*_{hom} are nucleation barriers for heterogeneous and homogeneous nucleation, respectively, and $f(\theta)$ is the wetting factor. b) Plot showing the wetting factor as a function of contact angle, in relation to the free energy change in the nucleation process. c) Optical images of a Galinstan droplet on a PDMS substrate before (left) and after (right) the HCl vapor treatment. d) Optical images and e) corresponding graph showing the contact angle of gallium droplets on various substrates. A smaller contact angle was observed with the graphene interface, indicating that a smaller free energy change is required to trigger the nucleation process. f) Comparison of the degree of supercoolings between bare gallium and graphene-coated gallium.

acid (HCl; 37 wt%) vapor for one minute, which was found to be an effective method for oxide layer removal.[23,24] Then, the contact angle of Galinstan on a glass substrate was measured before the contact angle of gallium was measured to ensure the reliability of the experiment[23] (Figure 2c). After treatment with HCl vapor, a liquid-like characteristic was observed on galinstan droplets, which resulted in an increase in contact angle (i.e., from 127.5° to 135.13°). A similar increasing trend was observed in the previous work by Kim et al.[23] (i.e., from 127.6° to 139.5°), validating the appropriateness of our experimental approach.

The contact angle of HCl-treated gallium was measured for four materials: glass, PDMS, RT623, and graphene (Figure 2d). Among these materials, graphene has the lowest contact angle of 124.7° while the remaining substrates have a contact angle of over 140° (Figure 2e), suggesting smaller interfacial free energy between graphene and gallium. To verify the performance of graphene in facilitating heterogeneous nucleation in gallium, the degree of supercooling for both bare gallium and graphene-coated gallium was measured in terms of the relationship between the contact angle and the nucleation energy barrier (Figure 2f). The results show that lowering the thawing temperature (T_{th}) decreases the degree of supercooling, and importantly, graphene, among other materials used in the experiment (Figure S2, Supporting Information), predominantly reduces the degree of supercooling of gallium, indicating its strong catalytic effect that can lead to accelerated liquid-to-solid transition.

We used the aforementioned feature of graphene to create a transformative platform with fast rigid–soft mode conversion. The development of the transformative platform involved the integration of 2D film-type graphene onto a gallium frame and encapsulation with silicone elastomer (**Figure 3**a). Through Raman spectroscopy (633 nm), it was confirmed that graphene was successfully transferred on top of gallium, as indicated by G and 2D peaks which represent the sp^2 hybridization of carbon atoms[25] (Figure 3b). The detailed fabrication process of the graphene-coated gallium transformative platform is illustrated in Figure 3c. A graphene layer on a copper substrate (Graphene Film, Graphenea, Inc.) was attached on water soluble tape, and a PMMA layer (150 nm in thickness), which worked as a carrier to transfer graphene onto a gallium frame,[26] was spincoated over the graphene-copper substrate. Then, after the water soluble tape was dissolved in water, the copper layer was etched and the graphene was transferred onto the gallium frame. Finally, the transformative platform was encapsulated with silicone (190 μm in thickness). Note that thinner silicone encapsulation is preferred to achieve a larger stiffness tuning ratio for transformative electronics. However, too thin encapsulating silicone can be torn easily, causing leakage of gallium. In our design, we used silicone material with high toughness (RT623, ELASTOSIL) to enable relatively thin encapsulation for leakage-free sealing of gallium.

One critical design parameter in TES operation is the stiffness tuning ratio. Figure 3d shows a fabricated transformative

© 2021 Wiley-VCH GmbH

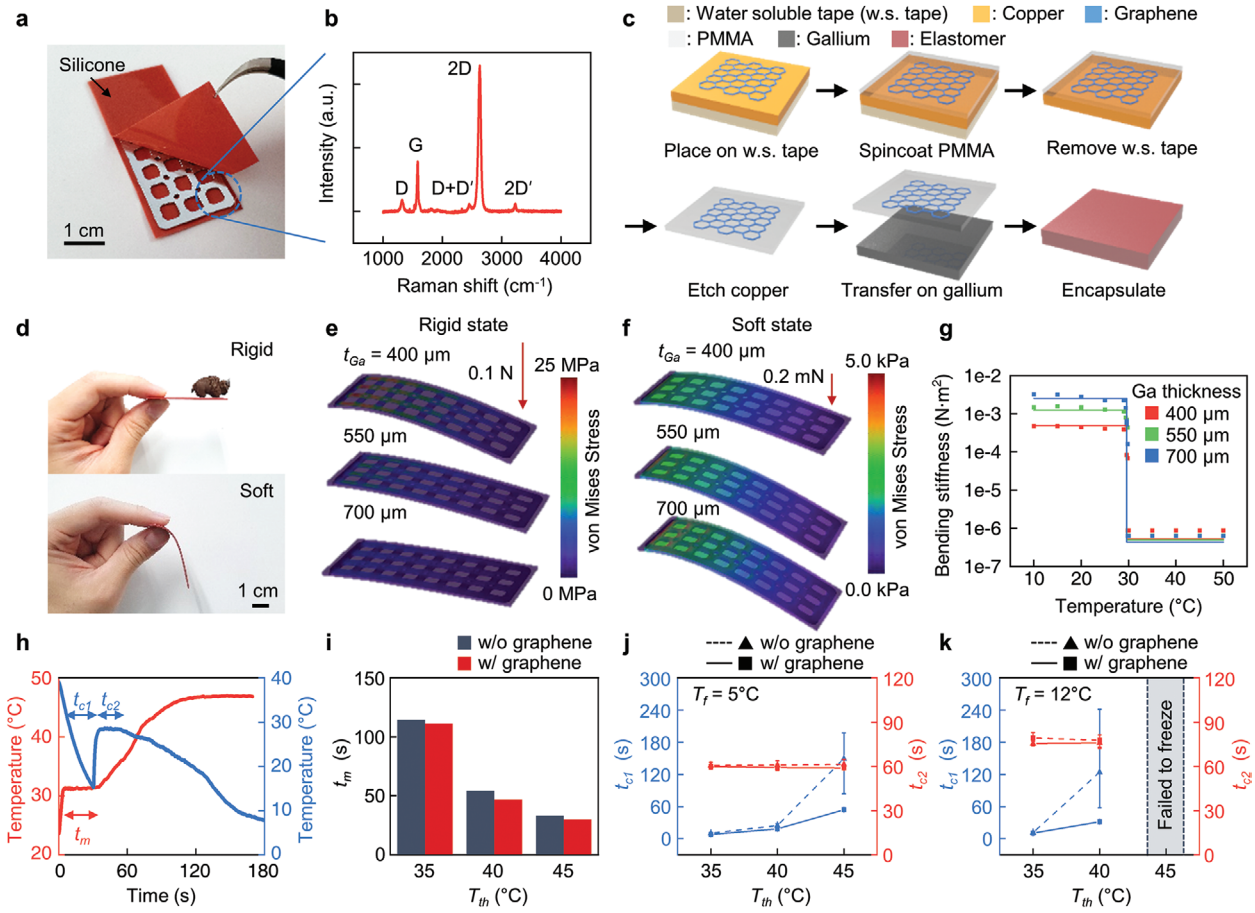

Figure 3. Characterization of a transformative platform built with a graphene-coated gallium frame. a) Optical image of a transformative platform. b) Raman spectrum of graphene-coated gallium at 633 nm excitation, showing successful integration of graphene with gallium. c) Schematic diagram illustrating the fabrication process of the transformative platform. d) Photographs of the resulting device in rigid (top) and soft (bottom) modes. e,f) FEA simulation of the bending stiffness of the device with various gallium thicknesses (400, 550, and 700 μm) in rigid (e) and soft (f) modes. g) Measured bending stiffness of the device as a function of temperature. The dots and solid lines in the plot indicate experimental data and simulation results in (e) and (f), respectively. h) Temperature changes of a device (550 μm-thick gallium frame encapsulated with 200 μm-thick silicone) during melting (red) and freezing (blue) processes. Note that the testbed platform was melted at a thawing temperature of 40 °C before freezing (blue). For its melting, the device was heated at the thawing temperature of 45 °C (red). i) Time required for the phase transition of gallium from rigid to soft state as a function of thawing temperature (T_{th}). j,k) Characteristic time required for phase transition of gallium from soft to rigid state with the application of freezing temperatures (T_f) of 5 °C (j) and 12 °C (k). Note that gallium thawed at 45 °C failed to be frozen at elevated temperature (12 °C) even with the integration of graphene (k), suggesting the need for low T_{th} (in case of operation with relatively high T_f) or an active cooling element that can offer substantially lower T_f (in case of operation with relatively high thawing temperature) for effective soft-to-rigid mode conversion.

platform with load-bearing ability when in rigid mode and pliability when in soft mode. Finite-element analysis (FEA) (Figure 3e,f) and an experiment (Figure 3g) were conducted to determine the variation in the bending stiffness of a transformative platform with a 150 μm-thick encapsulant and three different gallium thicknesses (i.e., 400, 550, and 700 μm; gallium frame width = 2 cm, length = 5 cm). As the gallium thickness was increased, the stiffness tuning ratio was enhanced (i.e., stiffness tuning ratio of 500, 2000, and 5000 for the frame with the thickness of 400, 550, and 700 μm, respectively). Considering that phase transition time increases as the gallium thickness increases, we chose 550 μm as the thickness of the gallium frame for our TES, which resulted in reasonably large stiffness variation (i.e., over three orders of magnitude) and fast transformation.

Understanding the thermal behavior of the transformative platform was also important to find the optimized operation conditions for rapid mode conversion. Figure 3h shows the typical melting and freezing behavior of gallium with the indicated characteristic times in its phase transition. In melting, the phase transition starts immediately when gallium reaches ≈30 °C and continues while the melting point is maintained (t_m: phase transition time required for melting). On the other hand, in freezing, the phase transition does not immediately occur even if the temperature of gallium reaches its freezing (melting) point due to supercooling. Instead, when gallium cools down to the nucleation temperature below its freezing point, the temperature sharply recovers to the freezing point and the phase transition starts. Here, we can define t_{c1} and t_{c2} as the characteristic time to reach the nucleation temperature and phase transition time, respectively.

© 2021 Wiley-VCH GmbH

According to the thermal characterization using an IR camera (Figure 3i), a higher thawing temperature (T_{th}) is advantageous to lessen t_m for speedy rigid-to-soft conversion and graphene shows a minimal effect on shortening t_m. For the soft-to-rigid conversion, to determine the effect of graphene on t_{c1} and t_{c2}, the transformative platform was heated with various T_{th} for 20 min and was frozen at 5 °C (Figure 3j) and 12 °C (Figure 3k). Experiments revealed that the effect of graphene was remarkable in reducing t_{c1} due to its influence on mitigating supercooling, but negligible for t_{c2}. Furthermore, a more profound effect on decreasing t_{c1} was observed for higher T_{th} cases. Nonetheless, overall, graphene-coated gallium thawed at a lower T_{th} showed a faster phase transition. Comparing Figure 3j,k, a lower freezing temperature resulted in a faster phase transition time, but this effect also became insignificant when the samples were thawed at 35 °C. Considering the fact that cooling of a device to below the room temperature would require external energy, for fast and energy-efficient soft-to-rigid conversion, it is desirable to operate a TES at the highest possible freezing temperature after softening it at T_{th} as low as 35 °C. However, this operation condition with a low T_{th} contradicts the requirement of high T_{th} for rapid rigid-to-soft transformation (Figure 3i). This issue can be overcome with an active temperature control strategy that applies a relatively high temperature (e.g., 45 °C) during the phase transition for melting (t_m) and decreases it to a low temperature (e.g., 35 °C) immediately after the completion of liquefaction to make the final temperature that gallium is subjected to during the softening process sufficiently low.

To enable such active temperature controls for fast-response transformation, we integrated an f-TED with a TES, which can act as a cooling and heating component based on the direction of the input current. The demonstration device, convertible between a rigid handheld display and flexible wearable display/pulsimeter, was built by incorporating an f-TED (1.3 mm-thick; Figure S3, Table S1,S2, Supporting Information) with the transformative platform shown in Figure 3 and flexible optoelectronics with LED arrays and a PD (Figure S4, Supporting Information), as illustrated in **Figure 4**a. The detailed fabrication process of the f-TED is presented in the Experimental Section and Figure S5 in the Supporting Information. Owing to the compliant structure of the f-TED, the f-TED-integrated TES device can be operated in rigid (Figure 4b) and flexible (Figure 4c) modes by controlling the stiffness of the transformative platform.

To ensure the stable performance of the f-TED under deformation, a bending test was conducted while its electrical resistance was measured. Figure 4d shows that the relative resistance changes of the f-TED are negligible (within 2% deviation up to a bending radius of 5 mm), demonstrating its operation stability in bending. Furthermore, the cyclic test result confirmed the durability of the f-TED (Figure 4e). To determine the operating conditions of the f-TED, its thermal characteristics were monitored during heating (Figure 4f) and cooling (Figure 4g) while various input currents were supplied to the f-TED. The red, green, blue, purple, and black lines represent the temperature changes induced with the input current of 1.4, 1.2, 1.0, 0.8, and 0.6 A, respectively. Note that the directions of the current are opposite for heating and cooling. In heating mode, the slope of the temperature change and steady-state temperature are proportional to the input current (Figure S6a, Supporting Information). On the contrary, in cooling mode, the minimum temperature decreases with the increase of the input current ($t < 40$ s in Figure 4g), but the input current shows no profound relationship with the steady-state temperature, which increases rapidly for current above 1.2 A (Figure S6b, Supporting Information). Based on these experimental results, for freezing of the gallium frame, we used 1.0 A to provide a consistently low temperature (i.e., the minimum temperature: 13.7 °C, steady-state temperature: 16.7 °C; Figure S7, Supporting Information), to rapidly overcome supercooling and to accelerate the phase transition.

Figure 4h shows the effect of the f-TED operation on the phase transition of gallium during rigid-to-soft conversion. It involves the use of the input current in the range of 0.6–1.4 A to the f-TED at room temperature which results in a phase transition around 30 °C. The red, green, blue, purple, and black lines represent the phase transition curves resulting from the input current of 1.4, 1.2, 1.0, 0.8, and 0.6 A, respectively. The phase transition time (t_m) decreases as the input current increases, i.e., a reduction of about 70% from ≈150 s at 0.6 A to ≈30 s at 1.4 A (Figure 4h,i). Considering the fact that a higher thawing temperature induces more severe supercooling in the freezing process, however, the input current should be lowered to 0.6 A after the phase transition (t_m = 30 s) with 1.4 A to maintain the temperature of gallium below 35 °C. This way, fast bidirectional rigid–soft conversion can be enabled as explained in the previous section. We used this operation scheme to prepare flexible TES samples for the study of thermal behavior of soft-to-rigid transition (Figure 4j, green and blue lines: bare and graphene-coated gallium without f-TED operation, respectively; red and black lines: bare and graphene-coated gallium with active cooling using the f-TED (the operation current of 1.0 A), respectively). Experimental results show that graphene effectively reduces the degree of supercooling (hence decreasing t_{c1}), and the f-TED further decreases time for soft-to-rigid conversion. More specifically, comparing the freezing processes of TESs built with graphene-coated gallium with and without the f-TED (black and blue lines in Figure 4j; ambient air, 22 °C), active cooling using the f-TED facilitated significant reduction in t_{c1} and t_{c2} (74% (from 19 to 5 s) and 53% (from 156 to 74 s) decreases, respectively; Figure 4k). Overall, the accelerating effects of the f-TED shortened the melting and freezing processes 91% (from 255 to 23 s) and 55% (from 175 to 79 s), respectively (Figure S8, Supporting Information) in comparison to the TES without f-TED (but with graphene-coated gallium), proving its critical role for accelerated bidirectional mode conversion. This TES shows consistent thermal behavior for rigid–soft mode conversion as demonstrated in our cyclic heating-cooling testing (Figure S9, Supporting Information), validating high reliability of the system.

Based on the operating conditions established in previous experiments, the TES shown in Figure 4a–c was implemented to convert between a rigid handheld display and a flexible wearable pulsimeter/display (Figure 4l). Note that in soft mode, the prototype can be used as either a wearable display by making the optoelectronics part face up (Figure 4l, bottom left) or a wearable pulsimeter by turning it upside down for monitoring

© 2021 Wiley-VCH GmbH

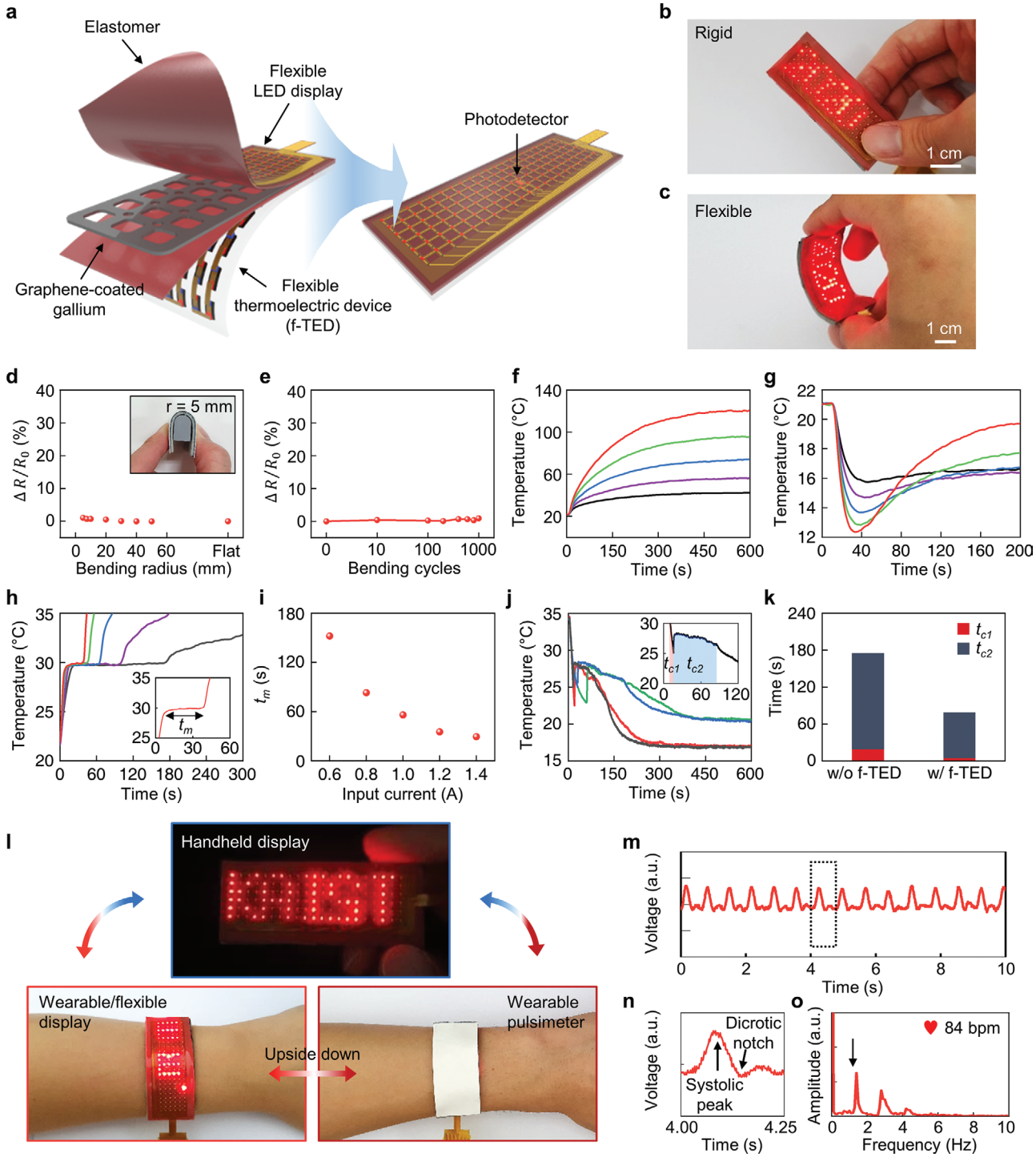

Figure 4. Proposed f-TED-integrated TES built on graphene-coated gallium that can covert between a rigid handheld display and a flexible wearable display or pulsimeter. a) Exploded-view schematic diagram that illustrates an integrated TES consisting of a flexible LED display, a transformative platform with graphene-coated gallium, and f-TED. b,c) Optical images of the TES in rigid (b) and flexible (c) modes. d) Relative resistance changes of the f-TED as a function of bending radius (r), demonstrating its stability under deformation. Here, R_0 is the resistance when the f-TED is flat. The inset shows an optical image of an f-TED bent with $r = 5$ mm. e) Cyclic bending test with $r = 10$ mm, showing its durability in dynamic operation. f,g) Temperature changes induced on the transformative platform when the f-TED is heating (f) or cooling (g) the device with the input current of 0.6 A (black), 0.8 A (purple), 1.0 A (blue), 1.2 A (green), and 1.4 A (red). h) Temperature changes of the transformative platform during the transition from rigid to flexible mode, driven by the f-TED with the input currents of 0.6 A (black), 0.8 A (purple), 1.0 A (blue), 1.2 A (green), and 1.4 A (red). The inset shows a magnified view of the red plot, highlighting the melting time (t_m) of gallium. i) Melting time as a function of the input current to the f-TED. j) Temperature changes of the transformative platform during the transition from flexible to rigid mode. The green and blue lines respectively indicate temperature changes of the platform made with bare gallium and graphene-coated gallium without f-TED activation. The red and black lines indicate

© 2021 Wiley-VCH GmbH

of blood pulse (Figure 4l, bottom right). Figure 4m shows the photoplethysmography (PPG) signal measured in the wearable pulsimeter mode. The systolic peak and the dicrotic notch are observed in the magnified view of a single pulse (Figure 4n), and Fourier transform analysis gives the peak value at 1.4 Hz indicating the heart rate of 84 bpm (Figure 4o). The proof-of-concept demonstration suggests practical and versatile utilities of the TES design, which may lead to a new development direction that can overcome limitations of both traditional rigid and flexible form of electronics.

In summary, TESs are an emerging class of electronics, which can broaden the utility of electronics by providing both rigid and soft forms through tuning of its shape and stiffness. The studies reported here established materials and electronics designs for a thermally-responsive TES capable of rapid bidirectional rigid–soft mode conversion. Graphene interfaced with the gallium-based TES platform significantly lowers the degree of supercooling in soft-to-rigid conversion. In addition, an integrated f-TED offers active temperature controls for acceleration of the overall phase transition process. The fast rigid–soft mode switching enabled by this scheme substantially enhances the pragmatic usefulness of the TES, overcoming the difficulty of achieving reliable bidirectional transformation in the previously reported TES.[9] Although the investigation focused on gallium-based TESs, the same general strategies can be applied to construct TESs with other liquid-solid phase change materials, such as fusible alloys,[27,28] for higher stiffness tuning and faster reconfiguration to open new opportunities for diverse real-world applications.

Experimental Section

Contact Angle Measurements: In this procedure, 12 µL gallium droplets were dispensed on various substrates (e.g., glass, PDMS, RT623, and graphene) using a syringe pump (NE-300, New Era Pump Systems, Inc). Glass substrates were prepared by rinsing glass slides (Product No. 1 000 412, Paul Marienfeld GmbH & Co. KG) with acetone and isopropyl alcohol (IPA) while other polymeric substrates (i.e., PDMS, RT623) were prepared through spin-casting. After the gallium droplets were dropped on the substrates, they were exposed to hydrogen chloride (HCl; 37 wt%) vapor for one minute to remove the oxide layer from the gallium surface; this layer naturally formed after gallium was dispensed from the syringe pump. Then, the contact angle was measured from photos taken using a digital camera (EOS 6D, Canon).

Fabrication of Transformative Platform with Graphene-Coated Gallium: A gallium frame was first created by casting and freezing liquid gallium (Ga metal 99.99, RotoMetals) on a PDMS mold with patterns. Subsequently, the gallium frame was detached from the mold. The periodic pattern with open holes was created in the gallium frame in order to not only confine gallium in relatively narrow encapsulating polymer channels to prevent accumulation of liquid gallium at specific corners, but also decrease the heat capacity of the gallium platform to enable fast temperature response. To transfer graphene onto the gallium frame, a monolayer graphene on a copper foil (Graphene Film, Graphenea, Inc) was attached on water soluble tape (ASWT-2, Aquasol). Then, a PMMA layer (150 nm in thickness) was spincoated over the graphene layer and cured at 150 °C for 15 min. The water soluble tape was removed by immersing it in water and the graphene layer on the exposed side was etched using oxygen plasma (50 sccm with 50 W for 10 min, KVIA-3008DC, KOREAVAC), while the foil was wet-etched. Finally, the graphene-layer covered with PMMA was transferred onto the gallium frame. The fabricated graphene-coated gallium was encapsulated with silicone elastomer (RT623 A/B, mixing ratio of 9:1). Note that there was an oxide layer between graphene and the gallium frame in the fabricated device. However, this oxide layer gets broken when making the initial solid-to-liquid transition of gallium and applying mechanical stress by deforming the device, thereby allowing direct contact of graphene with liquid gallium. Thus, it can give notable catalytic effect equivalent to the one induced in the gallium device where graphene was integrated on the gallium after the surface oxide removal using HCl vapor (Figure S10, Supporting Information).

Fabrication of f-TED: For the fabrication of the f-TED, copper was deposited and patterned on a polyimide film, and solder paste ($Sn_{96.5}Ag_{3.0}Cu_{0.5}$) was printed onto the copper patterns. Then, P- and N-type BiTe-based thermoelectric legs were mounted onto the solder and connected electrically in series and thermally in parallel, in a similar way implemented in a conventional rigid thermoelectric device.[29] Then, to make the device flexible, the rigid top and bottom plates were eliminated, and the empty space between the legs was filled with polymer aerogel with low thermal conductivity ($\approx$0.03 $W \cdot m^{-1} \cdot K^{-1}$)[30] as illustrated in Figure S5 in the Supporting Information. To create a flexible heatsink, an Al-contained silicone film (500 µm-thick) with high thermal conductivity ($\approx$2.2 $W\ m^{-1}\ K^{-1}$) was formed by screen-printing with a silicone paste (KE-3467, Shin-Etsu), and cured at 60 °C for 2 h in a convection oven. Finally, the flexible heatsink was bonded to the f-TED using thermal paste (PK-Zero Thermal Compound, Prolimatech, Inc) with thermal conductivity of 8.1 $W\ m^{-1}\ K^{-1}$.

Fabrication of a Multipurpose TES Device: To fabricate the TES shown in Figure 4, a transformative platform, a flexible optoelectronic device, and an f-TED were integrated as one unit. Red LEDs (624 nm; APG0603SEC-E-TT, Kingbright) and a photodetector (630 nm; ALS-PT19-315C/L177/TR8, Everlight Electronics) were mounted on a flexible circuit, which was constructed with copper interconnects (18 µm in thickness) on a Kapton film (120 µm in thickness). Finally, the fabricated flexible circuit and the f-TED were attached on the top and the bottom side of the transformative platform using silicone (Ecoflex 00-30, Smooth-On) as adhesives.

Mechanical Modeling and Analysis: For simulation of the bending stiffness of the transformative platforms in rigid and soft mode, a commercial FEA software (COMSOL Multiphysics, COMSOL, Inc) was used. Then 3D models of transformative platforms built with a gallium frame and silicone encapsulation (RT623, ELASTOSIL) were simulated using free tetrahedral mesh with force applied at the tip of the platform (Young's modulus of solid gallium = 9.8 GPa, Young's modulus of RT623 = 290 kPa). The applied forces for devices in rigid and soft mode were 0.1 N and 0.2 mN, respectively. Then, based on the simulated deflection values, the bending stiffnesses were calculated using the equation $\overline{EI} = FL^3 / 3\Delta z$, where $\overline{EI}$ is the bending stiffness, F is the applied force, L is the length of the transformative platform, and Δz is the deflection.

Measurement of Bending Stiffness: To measure the bending stiffness of the transformative platform, one end of the device sample was clamped, and the other end was deflected. For measurement in rigid mode, a 10-g weight was placed on the free end of the sample, and the resulting

the temperature changes of the platform built with bare gallium and graphene-coated gallium, respectively, with active cooling by the f-TED (operation current of 1.0 A). The inset shows a magnified view of the black plot, highlighting characteristic time (t_{c1}: time during supercooled state, t_{c2}: time for phase transition) required for freezing of gallium. k) Characteristic time needed for the flexible-to-rigid mode conversion of the TES without and with the f-TED. l) Application demonstration of multipurpose TES that can transform between a rigid handheld display (top) and a flexible wearable display (bottom left) or a pulsimeter (bottom right). m) Photoplethysmography (PPG) signal measured from the radial artery in the flexible wearable mode (l, bottom right). n) Magnified view of a single pulse signal in the black dashed box in (m). o) Fast Fourier transform (FFT) of PPG signal in (m).

© 2021 Wiley-VCH GmbH

deflections at different temperatures were measured using an optical camera. For measurement in soft mode, the sample was clamped closed to the free end and the deflections induced by the gravity were measured by varying temperatures. To control the ambient temperature, the experimental set-up was prepared in a constant temperature chamber (HQ-DTH, Coretech) and the temperature was increased from 10 °C to 50 °C by increasing the temperature at increments of 0.1 °C. Finally, the bending stiffnesses were calculated using the bending stiffness equation presented in Note S2 in the Supporting Information.

Experiments on Human Subjects: All experiments on human skins were performed under approval from Institutional Review Board at Korea Advanced Institute of Science and Technology (protocol number: KH2018-35) and received informed consent from the volunteer subjects.

Supporting Information

Supporting Information is available from the Wiley Online Library or from the author.

Acknowledgements

S.-H.B. and C.S.K. contributed equally to this work. This work was supported by the Basic Science Research Program through the National Research Foundation of Korea (NRF) funded by the Ministry of Science and ICT (NRF-2018R1C1B6001706 and NRF-2020M3C1B8A01111568 to J.-W.J.). This work was also supported by Samsung Electronics through Samsung Electronics-KAIST cooperation center.

Conflict of Interest

The authors declare no conflict of interest.

Keywords

bidirectional stiffness tuning, flexible thermoelectric devices, graphene, supercooling of gallium, transformative electronics

Received: October 22, 2020
Revised: December 6, 2020
Published online: January 25, 2021

[1] H. Lim, H. S. Kim, R. Qazi, Y. Kwon, J. Jeong, W. Yeo, *Adv. Mater.* **2020**, *32*, 1901924.
[2] J.-W. Jeong, W.-H. Yeo, A. Akhtar, J. J. S. Norton, Y.-J. Kwack, S. Li, S.-Y. Jung, Y. Su, W. Lee, J. Xia, H. Cheng, Y. Huang, W.-S. Choi, T. Bretl, J. A. Rogers, *Adv. Mater.* **2013**, *25*, 6839.
[3] M. Kaltenbrunner, T. Sekitani, J. Reeder, T. Yokota, K. Kuribara, T. Tokuhara, M. Drack, R. Schwödiauer, I. Graz, S. Bauer-Gogonea, S. Bauer, T. Someya, *Nature* **2013**, *499*, 458.
[4] S. Wang, J. Xu, W. Wang, G.-J. N. Wang, R. Rastak, F. Molina-Lopez, J. W. Chung, S. Niu, V. R. Feig, J. Lopez, T. Lei, S.-K. Kwon, Y. Kim, A. M. Foudeh, A. Ehrlich, A. Gasperini, Y. Yun, B. Murmann, J. B.-H. Tok, Z. Bao, *Nature* **2018**, *555*, 83.
[5] J.-W. Jeong, G. Shin, S. I. Park, K. J. Yu, L. Xu, J. A. Rogers, *Neuron* **2015**, *86*, 175.
[6] R. Qazi, A. M. Gomez, D. C. Castro, Z. Zou, J. Y. Sim, Y. Xiong, J. Abdo, C. Y. Kim, A. Anderson, F. Lohner, S.-H. Byun, B. Chul Lee, K.-I. Jang, J. Xiao, M. R. Bruchas, J.-W. Jeong, *Nat. Biomed. Eng.* **2019**, *3*, 655.
[7] J.-W. Jeong, J. G. McCall, G. Shin, Y. Zhang, R. Al-Hasani, M. Kim, S. Li, J. Y. Sim, K.-I. Jang, Y. Shi, D. Y. Hong, Y. Liu, G. P. Schmitz, L. Xia, Z. He, P. Gamble, W. Z. Ray, Y. Huang, M. R. Bruchas, J. A. Rogers, *Cell* **2015**, *162*, 662.
[8] K. N. Noh, S. I. Park, R. Qazi, Z. Zou, A. D. Mickle, J. G. Grajales-Reyes, K.-I. Jang, R. W. Gereau, J. Xiao, J. A. Rogers, J.-W. Jeong, *Small* **2018**, *14*, 1702479.
[9] S.-H. Byun, J. Y. Sim, Z. Zhou, J. Lee, R. Qazi, M. C. Walicki, K. E. Parker, M. P. Haney, S. H. Choi, A. Shon, G. B. Gereau, J. Bilbily, S. Li, Y. Liu, W.-H. Yeo, J. G. McCall, J. Xiao, J.-W. Jeong, *Sci. Adv.* **2019**, *5*, eaay0418.
[10] S.-H. Byun, J. Y. Sim, K.-C. Agno, J.-W. Jeong, *Mater. Today Adv.* **2020**, *7*, 100089.
[11] C. Zhang, L. Li, X. Yang, J. Shi, L. Gui, J. Liu, *Int. J. Heat Mass Transfer* **2020**, *148*, 119055.
[12] H. Kumano, T. Hirata, K. Mitsuishi, K. Ueno, *Int. J. Refrig.* **2012**, *35*, 1266.
[13] E. Miyasaka, M. Takai, H. Hidaka, Y. Kakimoto, I. Hirasawa, *Ultrason. Sonochem.* **2006**, *13*, 308.
[14] M. Kamalipour, S. A. M. Dehghani, A. Naseri, S. Abbasi, *J. Pet. Sci. Eng.* **2017**, *151*, 362.
[15] S. Park, N. Baugh, H. K. Shah, D. P. Parekh, I. D. Joshipura, M. D. Dickey, *Adv. Sci.* **2019**, *6*, 1901579.
[16] Y. Zhang, N. Zhang, H. Hingorani, N. Ding, D. Wang, C. Yuan, B. Zhang, G. Gu, Q. Ge, *Adv. Funct. Mater.* **2019**, *29*, 1806698.
[17] X. Li, Y. Chen, Z. Cheng, L. Jia, S. Mo, Z. Liu, *Appl. Energy* **2014**, *130*, 824.
[18] S. Karthika, T. K. Radhakrishnan, P. Kalaichelvi, *Cryst. Growth Des.* **2016**, *16*, 6663.
[19] A. I. Hienola, P. M. Winkler, P. E. Wagner, H. Vehkamäki, A. Lauri, I. Napari, M. Kulmala, *J. Chem. Phys.* **2007**, *126*, 094705.
[20] B. Cantor, *Philos. Trans. R. Soc., A* **2003**, *361*, 409.
[21] L. Jia, L. Peng, Y. Chen, S. Mo, X. Li, *Appl. Energy* **2014**, *124*, 248.
[22] W. Cui, L. Jia, Y. Chen, Y. Li, J. Li, S. Mo, *Nanoscale Res. Lett.* **2018**, *13*, 145.
[23] D. Kim, P. Thissen, G. Viner, D.-W. Lee, W. Choi, Y. J. Chabal, J.-B. Lee, *ACS Appl. Mater. Interfaces* **2013**, *5*, 179.
[24] G. Li, M. Parmar, D. Kim, J.-B. Lee, D.-W. Lee, *Lab Chip* **2014**, *14*, 200.
[25] A. C. Ferrari, D. M. Basko, *Nat. Nanotechnol.* **2013**, *8*, 235.
[26] X. Li, Y. Zhu, W. Cai, M. Borysiak, B. Han, D. Chen, R. D. Piner, L. Colombo, R. S. Ruoff, *Nano Lett.* **2009**, *9*, 4359.
[27] S. Yoshida, Y. Morimoto, L. Zheng, H. Onoe, S. Takeuchi, *Soft Rob.* **2018**, *5*, 718.
[28] L. Wang, Y. Yang, Y. Chen, C. Majidi, F. Iida, E. Askounis, Q. Pei, *Mater. Today* **2018**, *21*, 563.
[29] G. J. Snyder, E. S. Toberer, *Nat. Mater.* **2010**, *7*, 105.
[30] B. J. Cho, S. J. Kim, J. S. Shin, S. Yim, H. D. Choi, Y. Kim, C. S. Kim, J. H. We, *WO2017074003*, **2017**.

© 2021 Wiley-VCH GmbH